Characterization of crystallographic defects in $LaNiO_3$ through TEM image simulations

Author: Joan Carles Bastons Garcia.
*Departament d'Electrònica, Universitat de Barcelona**

Advisors: Sònia Estradé Albiol and Catalina Coll Benejam

Abstract: Lanthanum nickel oxide, $LaNiO_3$, is often used as an electrode in many electronic devices due to its low resistivity. The study of its properties requires understanding them in the nanoscale and, for this purpose, the electron transmission microscope is an indispensable tool. In the present work, we aim to examine the defects observed in High Angular Annular Dark Field (HAADF) images of a lanthanum nickel oxide thin film grown epitaxially on a lanthanum aluminate substrate. For this end, High Resolution Transmission Electron Microscopy (HRTEM) and HAADF images are simulated following the multislice method, implemented by *Temsim*, a software provided freely by E.J. Kirkland. Results show that the multislice method is a powerful tool so as to interpret the defects in the structure.

I. INTRODUCTION

After Louis de Broglie announced his theory that electrons could behave as waves in 1925 and electron-diffraction experiments were carried out, Knoll and Ruska built an electron microscope in 1932. The main advantage of electrons is that by increasing their energy, the electron wavelength gets smaller and, hence, resolution increases. Although there is a limitation for resolution due to the aberrations of the electromagnetic lenses, it is better than the resolution provided by light microscopes, in the order of 1nm compared to 0.1μm. Another main difference is that the transmission electron microscope obtains a final image based on diffraction effects and an intensity distribution, instead of direct observation through light. Many TEM techniques (HRTEM, STEM, EELS, etc.) have been developed in the last decades.

The main purpose of this project will be to examine and characterize some particular defects observed in HAADF images. To do so, we will make an assumption about these defects and, through simulations, we will verify if our hypothesis holds. Simulations will follow the multislice method, which consists in dividing the sample into thin slices and calculating the propagation of the electron wave through the specimen. Two types of simulations will be studied, HRTEM and HAADF image simulations, in order to compare the defects in both kinds of images and discuss the information that each technique provides. Besides, HAADF simulation will be compared with the experimental images of the defects obtained in the TEM.

The studied system is a lanthanum nickel oxide thin film grown on a lanthanum aluminate, LAO, substrate. The thickness of the $LaNiO_3$ film is 35nm and the first atomic layers over the substrate show full adaptation to the LAO structure with a reduction of the lattice parameter around 1%. However, beyond the first 3-5nm, defects arise like the ones shown in Figures 1 and 2.

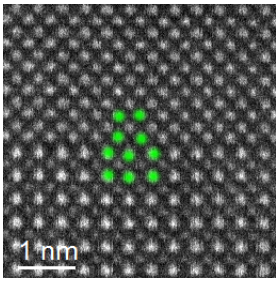

FIG. 1: HAADF image of $LaNiO_3$. The green points highlight the area of the defect.

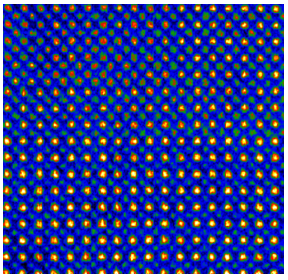

FIG. 2: HAADF image of $LaNiO_3$. The image has been colored for better appreciation.

The main goal of this project is to determine and characterize these defects. We will assume the hypothesis that they are atomic displacements (1/2, 1/2, 1/2) and, through simulations, this will be verified. These kind of defects are known as Ruddlesden-Popper faults.

II. IMAGING THROUGH TEM

The aim of TEM is to obtain an image of a sample based on its interaction with an electron beam. Each point of the object is associated with a small region in the final image, including overlapping between points. From a mathematical viewpoint, we can consider the specimen as a function $f(x, y)$ and the final image is a weighted contribution of each point, determined by a convolution. The point-spread function $h(\vec{r})$ represents the role of the microscope and describes how a point spreads into a disk. The final image $g(\vec{r})$ is the following convolution product:

$$g(\vec{r}) = f(\vec{r}) \otimes h(\vec{r}). \quad (1)$$

*Electronic address: jcbastonsgarcia@gmail.com

The general object transmission function can be assumed as

$$f(x,y) = A(x,y) \cdot e^{-i\phi_t(x,y)}, \tag{2}$$

where $A(x,y)$ is the amplitude and $\phi_t(x,y)$ is the phase, which depends on the thickness t of the specimen. Given an incident electron wave with energy E_0, the interaction with the sample can alter either their amplitude or their phase.

A. Phase contrast: HRTEM

We assume a thin sample, with a small thickness t, so that the 3D electrostatic potential can be approximated by a 2D projected one, calculated as

$$V_t(x,y) = \int_0^t V(x,y,z)dz. \tag{3}$$

Therefore, the electrons within the sample have an energy $E_0+V(x,y,z)$ at each position along the z-axis, that is, a change of the wavelength and, hence, a variation of their phase. The total phase shift is given by

$$\phi = \sigma \int_0^t V(x,y,z)dz = \sigma V_t(x,y), \tag{4}$$

where σ is the interaction constant. Since there is no amplitude shift, we assume $A = 1$, then the specimen transmission function is

$$f(x,y) = e^{-i\sigma V_t(x,y)-\mu(x,y)}, \tag{5}$$

where $\mu(x,y)$ refers to electron absorption and it is often omitted for thin samples. So far, we have expressed the specimen as a phase object, which is known as the weak phase-object approximation (WPOA) and it is only valid for thin specimens. Furthermore, in case of very thin specimens, the Taylor expansion of the exponential in Equation (5) can be truncated at first order. Consequently,

$$f(x,y) \approx 1 - i\sigma V_t(x,y). \tag{6}$$

Then, the convolution with the point-spread function is given by

$$g(x,y) = [1 - i\sigma V_t(x,y)] \otimes h(x,y). \tag{7}$$

The real intensity image is obtained by taking the squared modulus. The function $h(x,y)$ represents the whole optical system of the microscope, though it is mainly dominated by aberrations of the electromagnetic lenses of the TEM. In terms of its Fourier transform, its expression is given by

$$H(k) = e^{-i\chi(k)}, \tag{8}$$

$$\chi(k) = \pi\lambda k^2\left(\frac{1}{2}C_s\lambda^2k^2 - \Delta f\right). \tag{9}$$

C_s is the spherical aberration coefficient and Δf is the defocus. Physically, the defocus is the distance between the defocused image plane and the ideal Gaussian image plane, while the spherical aberration is related with the diameter of the disk that ideally would be a point object. Besides, C_s remains almost constant for a TEM at a given beam energy, whereas the defocus varies with the specimen and the strength of the lenses. Note also that Equation (9) is a truncated Taylor series on even powers of k, since the lenses are perfectly symmetric and, thus, do not depend on k_x or k_y. The next term of the series has as a coefficient the chromatic aberration coefficient, C_c. However, in case of thin samples, it is often neglected.

B. Amplitude contrast: HAADF

Amplitude contrast can be divided into two types: mass contrast and diffraction contrast. Mass contrast or Z-contrast consists in the elastic interaction of the electrons of the beam with the atomic nucleus. High Angular Annular Dark Field (HAADF) is an imaging technique based on mass-contrast in which electrons are scattered at high angles and collected in an annular detector. The scattering follows the Rutherford law and the expression of the Rutherford cross section at high angles is given by

$$\sigma_R = 1.62 \times 10^{-24}\left(\frac{Z}{E_0}\right)^2 cotg^2\left(\frac{\theta}{2}\right). \tag{10}$$

Note the dependence on the energy of the incident beam E_0 and the atomic number Z. This means that the probability of a scattering with the nucleus is higher for higher Z-specimens and at lower beam energies. HAADF has two remarkable advantages; the first one is that the final intensity only depends on Z and on the thickness of the specimen. Therefore, if the thickness is assumed constant, then the final image has atomic resolution, since it only depends on Z. The other advantage is that there are no contrast changes for small variations of the defocus.

III. IMAGE SIMULATION

As we said previously, simulations are a tool that provides an interpretation of the images obtained in TEM. There are two methods for simulating images: Bloch waves and the multislice method. The second one was proposed by Cowley and Moodie in the sixties and became more successful than the Bloch waves for efficient computational reasons. In the multislice approach, the specimen is divided into two-dimensional thin slices along the electron beam direction in order to apply the Weak Phase Object Approximation in the calculation of the

transmition function. Indeed, for each slice n, the projected atomic potential is calculated and so is the transmission function $t_n(x, y)$ as it follows

$$t_n(x, y) = \exp\big(i\sigma V_{t,n}(x, y)\big). \tag{11}$$

Moreover, the propagation function $p_n(x, y, \Delta z_n)$ describes the propagation of the electron wave from the nth slice to the next one, and it is calculated following the Fresnel diffraction.

A. HRTEM image simulation

HRTEM image simulation consists in the following steps. The incident function is initialized as $\psi_0(x, y) = 1$ and the wave function is determined recursively by

$$\psi_{n+1}(x, y) = p_n(x, y, \Delta z_n) \otimes [t_n(x, y)\psi_n(x, y)]. \tag{12}$$

By the Fourier convolution theorem,

$$\psi_{n+1}(\vec{x}) = FT^{-1}[p_n(\vec{x}, \Delta z_n)FT(t_n(\vec{x})\psi_n(\vec{x}))], \tag{13}$$

which simplifies the calculus due to the implementation of the Fast Fourier transform. Let $\psi_n(x, y)$ denote the final wave function. Then, it is convoluted with the transfer function of the objective lens $h(x, y)$, that is

$$\psi_i(\vec{x}) = \psi_n(\vec{x}) \otimes h(\vec{x}) = FT^{-1}[\psi_n(\vec{k})H(\vec{k})]. \tag{14}$$

Finally, the image intensity is obtained by taking the squared modulus,

$$g(x, y) = |\psi_i(\vec{x})|^2. \tag{15}$$

B. HAADF image simulation

HAADF image simulation is slightly different from HRTEM. As in the previous case, the sample is divided into thin slices. Thus, the projected atomic potential and the transmission function are calculated for each one. Since the electron wave interacts first with the lenses and afterwards with the sample, a probe function $\psi_p(\vec{x}, \vec{x_p})$ is initialized so that it includes the lenses effects, though it is only valid at position $\vec{x_p}$. Then, the wave function through the specimen is calculated by Equation (13). Finally, the image intensity at a point $\vec{x_p}$ is given by

$$g(\vec{x_p}) = \int D(\vec{k})|\psi_n(\vec{k}, \vec{x_p})|^2 d^2(\vec{k}), \tag{16}$$

where $D(\vec{k})$ is a function that takes the value 1 on the annular detector, otherwise it is zero. Repeating the process for each point or pixel, the whole image is obtained. Since the calculus is done pixel by pixel, simulation requires time-consuming computation. Therefore, the expression

$$N_x, N_y \gtrsim 2a\frac{\theta_d}{\lambda} \tag{17}$$

provides us a choice of the number of pixels so that aliasing is avoided and the image is obtained in a reasonable time (order of days). In the expression, a refers to the dimension of the super-cell, θ_d to the detector angle (averaged) and λ the wavelength of the incident electrons.

IV. $LaNiO_3$

Lanthanum nickel oxide, $LaNiO_3$, is an oxide that belongs to the perovskite nickelates family. Regarding its atomic structure, the unit cell is cubic with a lattice parameter $a = 3.83$Å.

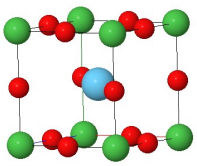

FIG. 3: Unit cell of $LaNiO_3$. The atom in blue is lanthanum, the red ones are oxygen and the green ones are nickel.

As Figure 3 shows, a lanthanum atom is placed at the center of the cubic cell. Four nickel atoms are placed at the vertex of the cube and eight oxygen atoms are placed at the middle of the edges.

One remarkable characteristic of this perovskite nickelate is its low resistivity, below $100\mu\Omega \times$ cm, and that is not affected by the metal-insulator transition, remaining a metal at all temperatures. Besides, as we said at the beginning, $LaNiO_3$ can grow in fully strained epitaxial thin films on a LAO substrate. This means that $LaNiO_3$ adopts the structure of the substrate and, consequently, the lattice parameter varies. In this particular case, the lattice parameter is $a = 3.79$Å. A variation of the lattice parameter could improve resistivity and, hence, improve $LaNiO_3$ as an efficient electrode in devices such as LEDs, lasers, etc.

V. RESULTS

According to Z-contrast, in Figures 1 and 2 each spot is identified as an atomic column and the brightest ones correspond to higher Z elements. Therefore, Figure 1 shows a vertical loss of the atomic column contrast related to the positions of lanthanum and nickel atoms. Figure 2 shows the same loss of atomic column contrast in the upper left corner. Next, in order to characterize these defects, we will carry out the simulations, assuming Ruddlesden-Popper faults in both cases.

First of all, we need to create a file specifying the position of each atom of the sample that we are about to simulate. To do so, a software from the University of Cádiz, which provides an easy way of constructing unit

cells and super-cells, has been used. It is also remarkable that this software includes the possibility to set the orientation, since the study of defects requires specifying the direction of the incident electron beam. Two super-cells, shown in Figure 4 and Figure 5, were built with dimension $60 \times 60 \times 60 \text{Å}^3$. In Figure 4, the super-cell has a displacement (1/2, 1/2, 1/2) along the direction [0 1 1] and the electron beam penetrates perpendicular to the indicated face, direction [001]. In Figure 5, the super-cell has a displacement (1/2, 1/2, 1/2) in a small region and the electron beam penetrates following the direction [001].

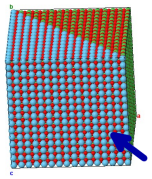

FIG. 4: Super-cell with a displacement (1/2, 1/2, 1/2) in direction [0 1 1].

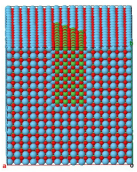

FIG. 5: Super-cell with a displacement (1/2, 1/2, 1/2) in a small region.

Once the super-cells are built, they can be simulated using the software *Temsim*, provided by E. J. Kirkland. This program implements the multislice method using a C++ code.

A. Simulated images

The first two simulated images were HRTEM images. The energy of the incident electron beam was $200keV$ and the slice thickness considered was set at 2Å, since it is approximately the distance between consecutive atomic planes.

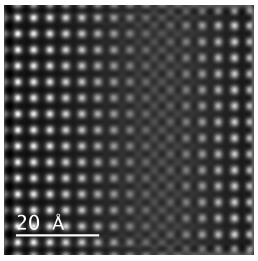

FIG. 6: HRTEM simulated image of the super-cell in Figure 4 with a defocus $\Delta f = 300$Å.

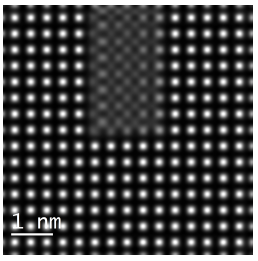

FIG. 7: HRTEM simulated image of the super-cell in Figure 5 with a defocus $\Delta f = 350$Å.

Both images show an asymmetry due to the displacements (1/2, 1/2, 1/2). Besides, the superposition regions have a diminution of contrast, which allows us to identify its shape, especially in Figure 7. The choice of the value for the defocus was taken so as to have well-focused images while the value for spherical aberration was given by the microscope, $C_s = 0.3$mm. If there had been available experimental images, the best defous would have been chosen by matching simulations with experimental images.

With the software *Temsim*, HAADF images of the two super-cells were simulated. According to experimental data, the beam energy was $E_0 = 200keV$, the spherical aberration was $C_s = 0.3$mm, the chromatic aberration was neglected and the objective aperture was fixed at 11.43mrad. The angles of the detector were assumed to be between 74mrad and 300mrad. In order to avoid aliasing, a 512×512 pixels sample of specimen transmission function was set. The probe wave function had a size of 1024×1024 pixels and the final image had a size of 256×256 pixels. The slices were 2Å thick, since this is approximately the interplanar distance.

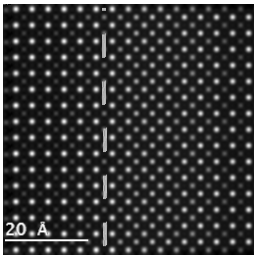

FIG. 8: HAADF simulated image of the super-cell in Figure 4.

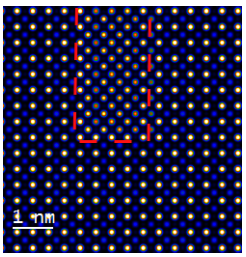

FIG. 9: HAADF simulated image of the super-cell in Figure 5.

As it can be observed, both images consist of clear spots that allow us to identify the displaced regions. Since HAADF is based on Z-contrast, each spot is identified with an atomic column and, even more, the brightest spots correspond to higher Z elements, in our case lanthanum. Therefore, the displacement of the brightest spots implies an atomic displacement. This reasoning is the main difference between HAADF and HRTEM simulated images, given that in phase contrast we cannot interpret the spots as atomic columns in the sample. In fact, the variation of the defocus in HRTEM images makes atoms appear either bright or dark. To sum up, from HRTEM images we cannot extract chemical information and, consequently, HRTEM provides qualitative information as a first approach (shape of the defect, extension, etc.). On the other hand, HAADF not only reveals structural information, but also chemical information with atomic resolution.

B. Comparison with the experimental images

In this section, we compare HAADF simulations with experimental images. We begin with Figure 4.

The images in Figure 10 show a displacement of the bright spots, lanthanum atoms according to Z-contrast. As we move upwards following lanthanum atomic columns, in a middle position we can appreciate a shift. Basically, the previous atomic planes disappear and

new ones appear between them. Therefore, the match of defects in simulated and experimental images confirms the thesis that there is a region of the sample where a plane is missing, causing a displacement (1/2, 1/2, 1/2) along the direction $[0, 1, 1]$. Hence, a Ruddlesden-Popper fault explains Figure 1.

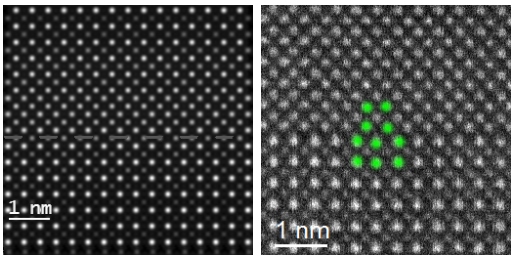

FIG. 10: The left-hand side image corresponds to the simulation of the super-cell in Figure 4 (rotated 90°) and, on the right-hand side, we have Figure 1.

Next, we examine the image in Figure 2.

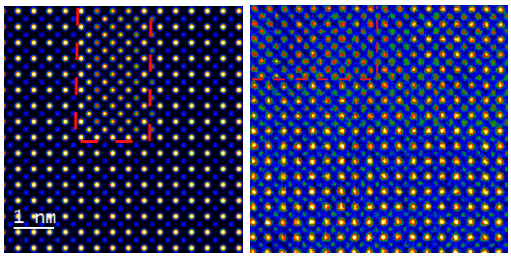

FIG. 11: The left-hand side image corresponds to the simulation of the super-cell in Figure 5 and, on the right-hand side, we have Figure 2.

Note that the region of the defaults in the simulated image is placed differently from the experimental one. In both images we observe that the columns and rows formed by the brightest spots, corresponding to lanthanum atoms, have a slightly less bright continuation inside the region of the defect due to a thickness diminution. Inside these regions, we also observe an additional bright column between two consecutive bright columns. They correspond to the (1/2, 1/2, 1/2) displaced lanthanum atomic planes according to the super-cell in Figure 5. Intensity differences between the two images could be due to the fact that the simulation may not assume the same displaced thickness that was present in the studied sample. From the HAADF image simulation we can conclude that a Ruddlesden-Popper fault explains the features in Figure 2.

VI. CONCLUSIONS

- A $LaNiO_3$ thin film grown on a LAO substrate was examined through HAADF in the TEM. In the images, some regions showed no lanthanum and nickel atomic column contrast. Ruddlesden-Popper faults were proposed to account for the lack of contrast. This assumption was checked through simulations.
- The multislice method was used for simulating HRTEM and HAADF images. One of the main difficulties was to find a HAADF simulated image which could be compared to the experimental one. Indeed, there are many factors to adjust, from defocus to the super-cell built, and the time-consuming computation limited the number of attempts that could be done.
- We obtained simulated images that provided an interpretation of the defects as Ruddlesden-Popper faults. We also compared HAADF and HRTEM simulations, and we concluded that, for characterizing the defects, HAADF simulations were more appropriated, since their interpretation is more straightforward.
- Further work should obtain HRTEM images of the sample and compare them with the HRTEM simulations that were carried out.

Acknowledgments

I would like to express my gratitude to Dr. Sònia Estradé for her guidance and advice. Also, my gratitude to the LENS-MIND-IN2UB group, especially to Catalina Coll, Dr. Lluís López and Dr. Francesca Peiró, for their help in carrying out this work.

I am also grateful to my parents and my sister for their support in all aspects not only while carrying out this project, but also through these years. Finally, I also thank the support received from my friends.

[1] John M. Cowley, *Diffraction physics*, Elsevier, Amsterdam, 3rd. edition, 1995.
[2] Earl J. Kirkland, *Advanced Computing in Electron Microscopy*, Springer, New York, 2nd edition, 2010.
[3] Earl J. Kirkland, *Temsim software*, `http://people.ccmr.cornell.edu/~kirkland/`
[4] Lluís López Conesa, PhD. Thesis, University of Barcelona, 2015.
[5] R. Scherwitzl, P. Zubko, C. Lichtensteiger and J.M. Triscone, "Electric-field tuning of the metak-insulation transition of ultrathin films of $LaNiO_3$", *Applied Physics Letters*, vol. 95, no. 22, pp. 10-13, 2009.
[6] David B. Williams and C. Barry Carter, *Transmission Electron Microscope: A Textbook for Material Science*, Springer, New York, 2nd. edition, 2009.